

# Northumbria Research Link

Citation: Bruno, Agostino Walter, Gallipoli, Domenico and Mendes, Joao (2022) Hydromechanical behaviour of two unsaturated silts: laboratory data and model predictions. Canadian Geotechnical Journal, 59 (6). pp. 837-846. ISSN 0008-3674

Published by: Canadian Science Publishing

URL: <https://doi.org/10.1139/cgj-2021-0170> <<https://doi.org/10.1139/cgj-2021-0170>>

This version was downloaded from Northumbria Research Link: <http://nrl.northumbria.ac.uk/id/eprint/46819/>

Northumbria University has developed Northumbria Research Link (NRL) to enable users to access the University's research output. Copyright © and moral rights for items on NRL are retained by the individual author(s) and/or other copyright owners. Single copies of full items can be reproduced, displayed or performed, and given to third parties in any format or medium for personal research or study, educational, or not-for-profit purposes without prior permission or charge, provided the authors, title and full bibliographic details are given, as well as a hyperlink and/or URL to the original metadata page. The content must not be changed in any way. Full items must not be sold commercially in any format or medium without formal permission of the copyright holder. The full policy is available online: <http://nrl.northumbria.ac.uk/policies.html>

This document may differ from the final, published version of the research and has been made available online in accordance with publisher policies. To read and/or cite from the published version of the research, please visit the publisher's website (a subscription may be required.)



**Northumbria  
University**  
NEWCASTLE



**UniversityLibrary**

1 **Hydromechanical behaviour of two unsaturated silts: laboratory data and model**  
2 **predictions**

3 Agostino Walter Bruno<sup>1</sup>, Domenico Gallipoli<sup>2</sup> and Joao Mendes<sup>3</sup>

4 <sup>1</sup> School of Engineering, Geotechnics and Structures, Newcastle University, Newcastle upon Tyne, United Kingdom.

5 <sup>2</sup> Dipartimento di Ingegneria Civile, Chimica e Ambientale, Università degli Studi di Genova, Genoa, Italy.

6 <sup>3</sup> Faculty of Engineering and Environment, Department of Mechanical & Construction Engineering, Northumbria  
7 University, Newcastle upon Tyne, United Kingdom.

8

9 DATE OF SUBMISSION: 24/06/2021

10 NUMBER OF WORDS: 5773

11 NUMBER OF TABLES: 5

12 NUMBER OF FIGURES: 13

13 CORRESPONDING AUTHOR: Agostino Walter BRUNO

14 Newcastle University

15 School of Engineering – Geotechnics and Structures

16 Devonshire Terrace

17 Drummond Building, Room 2.19

18 NE1 7RU, Newcastle upon Tyne

19 United Kingdom

20 e-mail: [agostino.bruno@newcastle.ac.uk](mailto:agostino.bruno@newcastle.ac.uk)

21

22 ***ABSTRACT:***

23 This paper presents the results from a campaign of unsaturated and saturated isotropic tests performed  
24 on two compacted silts of different coarseness, namely a clayey silt and a sandy silt, inside triaxial  
25 cells. Some tests involved an increase/decrease of mean net stress at constant suction or an  
26 increase/decrease of suction at constant mean net stress. Other tests involved an increase of mean net  
27 stress at constant water content with measurement of suction. During all tests, the void ratio and  
28 degree of saturation were measured to investigate the mechanical and retention behaviour of the soil.  
29 The experimental results were then simulated by the bounding surface hydromechanical model of  
30 Bruno and Gallipoli (2019), which was originally formulated to describe the behaviour of clays and  
31 clayey silts. Model parameters were calibrated against unsaturated tests including isotropic loading  
32 stages at constant water content with measurement of varying suction. Loading at constant water  
33 content is relatively fast and allows the simultaneous exploration of large ranges of mean net stress  
34 and suction, thus reducing the need of multiple experiments at distinct suction levels. Predicted data  
35 match well the observed behaviour of both soils, including the occurrence of progressive yielding and  
36 hysteresis, which extends the validation of this hydromechanical model to coarser soils. Specific  
37 features of the unsaturated soil behaviour, such as wetting-induced collapse, are also well reproduced.

38 ***KEYWORDS:***

39 Unsaturated soils; hydromechanical behaviour; bounding surface plasticity; unsaturated triaxial  
40 testing; collapse-compression.

41

42

43

44 ***INTRODUCTION***

45 Geotechnical design often requires the prediction of the hydromechanical behaviour of unsaturated  
46 soils as these make up a large proportion of earthworks including fills, embankments and dams.  
47 Shallow natural soils also exist in a partly saturated state, which has important consequences on the  
48 stability of foundations, cuttings and slopes.

49 Over the past decades, researchers have developed reliable techniques to measure the hydraulic and  
50 mechanical behaviour of unsaturated soils by upgrading standard equipment for saturated soils such  
51 as oedometers, shear boxes and triaxial cells (e.g. Gan et al., 1988; Delage et al., 1998; Cunningham  
52 et al., 2003; Tarantino and Tombolato, 2005; Jotisankasa et al., 2007) or by designing new  
53 instrumentation such as pressure plates, psychrometers and high-capacity tensiometers (e.g. Fredlund  
54 and Wong, 1989; Ridley and Burland, 1993; Tinjum et al., 1997; Mendes et al., 2008; Lourenço et  
55 al., 2008; Lourenço et al., 2011; Toll et al., 2013; Mendes et al., 2019).

56 These experimental advances have in turn elicited the development of increasingly accurate material  
57 models. A milestone has been the definition of the soil-water retention curve linking uniquely the  
58 degree of saturation to pore water suction (e.g. Van Genuchten, 1980; Fredlund and Xing, 1994),  
59 which has found application not only in geotechnical engineering but also agriculture and hydrology  
60 (Siemens et al., 2014; Balzano et al., 2021). More complex retention laws have also been proposed  
61 to describe the effects of hysteresis, material fabric and volumetric deformations on soil saturation  
62 (e.g. Gallipoli et al., 2003a; Nuth and Laloui, 2008; Tarantino, 2009; Romero et al., 2011) while  
63 mechanical laws have been formulated to describe the effect of pore water capillarity on soil stiffness,  
64 deformation and strength (e.g. Alonso et al., 1990; Wheeler and Sivakumar, 1995; Gallipoli et al.,  
65 2003b; Lim and Siemens, 2016). In some instances, retention and mechanical laws have been  
66 combined into a single coupled hydromechanical framework (e.g. Wheeler et al., 2003; Khalili et al.,

67 2008; Sun et al., 2008; Lloret-Cabot et al., 2013; Sun et al., 2016; Lloret-Cabot et al., 2017; Lloret-  
68 Cabot et al., 2018; Zhou et al., 2018).

69 Past research has tended to focus on the behaviour of unsaturated clays while coarser soils have  
70 generally received less attention (Delage et al., 1996; Geiser et al., 2006; Oka et al., 2010; Zhao and  
71 Zhang, 2014). A thorough understanding of coarser soils is, however, important as these materials  
72 are commonly encountered in geotechnical works (e.g. dams, embankments) and widely used in earth  
73 building (Bruno et al., 2017; Cuccurullo et al., 2018). This paper contributes to the investigation of  
74 the unsaturated behaviour of coarser soils by testing two different silts under isotropic conditions  
75 inside triaxial cells along a variety of stress paths that include: a) increase/decrease of mean net stress  
76 at constant suction, b) increase/decrease of suction at constant mean net stress and c) increase of mean  
77 net stress at constant water content with the simultaneous measurement of suction. Recall that the  
78 mean net stress,  $p_{net}$  is the difference between the mean total stress,  $p$  and the pore air pressure,  $u_a$   
79 while the suction,  $s$  is the difference between the pore air pressure,  $u_a$  and the pore water pressure,  
80  $u_w$ . Note that the present experimental campaign focuses on remoulded/compacted samples whereas  
81 the characterisation of intact/undisturbed soils is outside the scope of this work.

82 Test results were used to calibrate the bounding surface model of Bruno and Gallipoli (2019), which  
83 predicts the hysteretic hydromechanical behaviour of unsaturated soils under isotropic stress states.  
84 The model accounts for the effect of hydraulic hysteresis and deformation on soil-water retention  
85 and, vice versa, for the effect of the degree of saturation and capillarity on deformation. Model  
86 parameters were calibrated against isotropic tests on unsaturated samples, which involved loading at  
87 constant water content with measurement of varying suction, followed by unloading at constant  
88 suction with measurement of varying water content. Note that loading at constant water content  
89 produces simultaneous variations of mean net stress and suction, which simplifies model calibration  
90 as it reduces the need of performing multiple tests at distinct suction levels. The calibrated model was

91 finally employed to simulate the soil response during additional tests not used for selecting parameter  
92 values. The simulations show a good agreement between predicted and experimental data, including  
93 the occurrence of collapse-compression upon wetting. This confirms that the model of Bruno and  
94 Gallipoli (2019) is indeed capable of describing the behaviour of relatively coarse materials, such as  
95 sandy silts, in addition to the behaviour of fine soils.

## 96 ***HYDROMECHANICAL MODEL***

97 The hydromechanical model of Bruno and Gallipoli (2019) couples the hysteretic retention law for  
98 deformable soils of Gallipoli et al. (2015) with the hysteretic mechanical law for unsaturated soils of  
99 Gallipoli and Bruno (2017), which are both briefly summarised in this section.

100 The retention law accounts for the combined effect of void ratio  $e$  and matric suction  $s$  on the  
101 hysteretic variation of degree of saturation  $S_r$  by means of two distinct equations, i.e. one for wetting  
102 and one for drying (Gallipoli et al., 2015). Similarly, the mechanical law accounts for the effect of  
103 degree of saturation  $S_r$  and mean average skeleton stress  $p' = p - u_a + S_r s$  (also known as Bishop's  
104 stress) on the hysteretic variation of void ratio  $e$  by means of two distinct equations, i.e. one for  
105 loading and one for unloading (Gallipoli and Bruno, 2017). Each one of the wetting, drying, loading  
106 and unloading equations originates from the integration of a differential constitutive law (Gallipoli et  
107 al., 2015; Gallipoli and Bruno, 2017) and, therefore, includes a constant of integration whose value  
108 must be determined by imposing a boundary condition. Table 1 summarises the above four equations  
109 together with the expressions of the respective constants of integration. Table 1 also lists the twelve  
110 parameters of the hydromechanical model, i.e. seven parameters for the retention law and five  
111 parameters for the mechanical law.

112

113

**Table 1.** Retention and mechanical laws

<b>Retention law (Gallipoli et al., 2015)</b>	
Wetting paths	$(S_r)_w = \left( 1 + \left( \frac{\left( s e^{\frac{1}{\lambda_s}} \right)^{\beta_w}}{\omega_w^{\beta_w} \left( 1 + C_w \left( s e^{\frac{1}{\lambda_s}} \right)^{\beta_w} \right)} \right)^{\frac{\lambda_s}{\beta_w m_w}} \right)^{-m_w}$
Wetting path – Constant of integration	$C_w = \frac{1}{\omega_w^{\beta_w}} \left( S_{r,0}^{-\frac{1}{m_w}} - 1 \right)^{-\frac{\beta_w m_w}{\lambda_s}} - \frac{1}{\left( s_0 e^{\frac{1}{\lambda_s}} \right)^{\beta_w}}$
Drying paths	$(S_r)_d = \left( 1 + \left( \frac{\left( s e^{\frac{1}{\lambda_s}} \right)^{\beta_d} + C_d}{\omega_d^{\beta_d}} \right)^{\frac{\lambda_s}{\beta_d m_d}} \right)^{-m_d}$
Drying path – Constant of integration	$C_d = \omega_d^{\beta_d} \left( S_{r,0}^{-\frac{1}{m_d}} - 1 \right)^{\frac{\beta_d m_d}{\lambda_s}} - \left( s_0 e^{\frac{1}{\lambda_s}} \right)^{\beta_d}$
Model parameters	$\lambda_s, \omega_w, m_w, \beta_w, \omega_d, m_d, \beta_d$
<b>Mechanical law (Gallipoli and Bruno, 2017)</b>	
Loading paths	$e = \left( \left( \frac{p' S_r^{\frac{\lambda_r}{\lambda_p}}}{\bar{p}_{ref}} \right)^{\gamma} + C_l \right)^{\frac{\lambda_p}{\gamma}}$
Loading paths – Constant of integration	$C_l = e_0^{-\frac{\gamma}{\lambda_p}} - \left( \frac{p'_0 S_{r,0}^{\frac{\lambda_r}{\lambda_p}}}{\bar{p}_{ref}} \right)^{\gamma}$
Unloading paths	$e = \frac{C_u}{\left( p' S_r^{\frac{\lambda_r}{\lambda_p}} \right)^{\kappa}}$
Unloading paths – Constant of integration	$C_u = e_0 \left( p'_0 S_{r,0}^{\frac{\lambda_r}{\lambda_p}} \right)^{\kappa}$
Model parameters	$\lambda_p, \lambda_r, \bar{p}_{ref}, \gamma, \kappa$

115 The constants of integration  $C_w$  and  $C_d$  uniquely identify the wetting and drying paths, respectively,  
116 passing through a soil state characterised by suction  $s_0$ , void ratio  $e_0$  and degree of saturation  $S_{r,0}$ .  
117 Similarly, the constants of integration  $C_l$  and  $C_u$  uniquely identify the loading and unloading paths,  
118 respectively, passing through a soil state characterised by void ratio  $e_0$ , mean average skeleton stress  
119  $p'_0$  and degree of saturation  $S_{r,0}$ . Further details about the derivation of both the retention and  
120 mechanical laws, together with a discussion of the physical meaning of the corresponding parameters,  
121 can be found in Gallipoli et al. (2015) and Gallipoli and Bruno (2017), respectively.

122 The above retention and mechanical laws are coupled via the iterative algorithm of Bruno and  
123 Gallipoli (2019). According to this algorithm, the degree of saturation computed from the retention  
124 law is inserted into the mechanical law to calculate the corresponding value of void ratio, which is  
125 then inserted back into the retention law to calculate a new value of degree of saturation. This triggers  
126 a recursive process, which is repeated n-times until the following two convergency criteria are  
127 simultaneously met:

$$\left| \frac{S_{r,n} - S_{r,n-1}}{S_{r,n-1}} \right| \leq 0.001 \quad (1a)$$

$$\left| \frac{e_n - e_{n-1}}{e_{n-1}} \right| \leq 0.001 \quad (1b)$$

128 Once Equations (1a) and (1b) are satisfied, the algorithm is assumed to have converged and the  
129 simulation moves to the next values of suction and mean net stress along the chosen path. Additional  
130 details about this iterative procedure can be found in Bruno and Gallipoli (2019).

131 This coupled hydromechanical framework has already been validated by Bruno and Gallipoli (2019)  
132 against laboratory data for fine soils whereas, in the present paper, the capabilities of the model are  
133 further tested against the behaviour of coarser materials.

134

135 **MATERIALS AND METHODS**

136 **Material properties**

137 The soils tested in the present work were provided by two brickwork factories, i.e. Nagen and  
 138 Bouisset, in the region of Toulouse (France). The grain size distributions of both soils were  
 139 determined by wet sieving and sedimentation according to the norms XP P94-041 (AFNOR, 1995)  
 140 and NF P 94-057 (AFNOR, 1992), respectively. The plasticity properties of the fine fraction (i.e. the  
 141 fraction passing through the 400  $\mu\text{m}$  sieve) were determined according to the norm NF P94-051  
 142 (AFNOR, 1993). The specific gravity of the soil grains,  $G_s$ , was instead measured by means of the  
 143 pycnometer test according to the norm NF P 94-054 (AFNOR, 1991). The clay activity,  $A$  (defined  
 144 as the ratio between the plasticity index and the soil fraction smaller than 2  $\mu\text{m}$ ) is equal to 0.79 for  
 145 the Nagen soil and 0.6 for the Bouisset soil, which classifies the former material as normally active  
 146 and the latter material as inactive (Skempton, 1953). This is also consistent with the mineralogical  
 147 data provided by the suppliers, which indicate a predominantly illitic content with a small quantity of  
 148 montmorillonite for the Nagen soil and a predominantly kaolinitic content for the Bouisset soil. Table  
 149 2 summarises the main properties of both materials.

**Table 2.** Main material properties

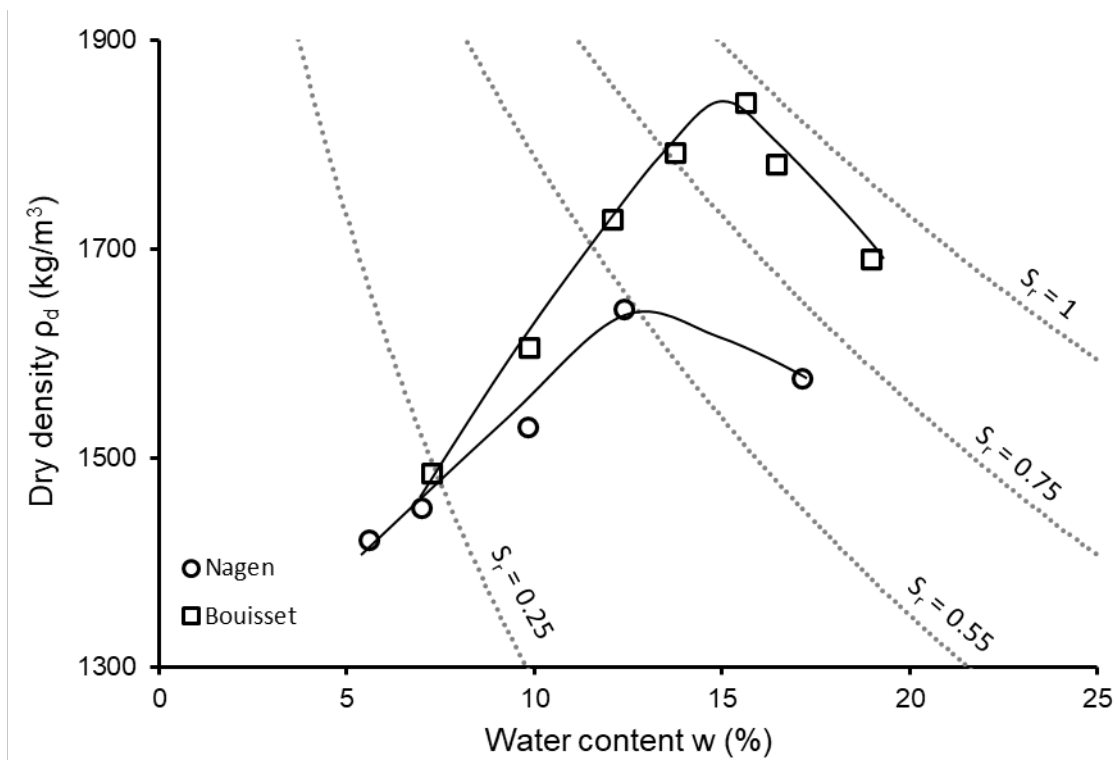
<b>Grain size distribution</b>		<b>NAGEN</b>	<b>BOUISSET</b>
Gravel	> 2 mm	0.4 %	0.0%
Sand	0.063 – 2 mm	40.4 %	26.6%
Silt	0.002 – 0.063 mm	42.9 %	41.9%
Clay	< 0.002 mm	16.3 %	31.5%
<b>Plasticity properties</b>			
	Liquid limit, $w_L$	33.0 %	35.5%
	Plastic limit, $w_P$	20.1 %	16.7%
	Plasticity index, $I_p$	12.9 %	18.8%
	Clay activity, $A$ (-)	0.79	0.60
<b>Specific gravity of soil grains</b>			
	Specific gravity, $G_s$ (-)	2.66	2.65

150 The compaction curves, relating dry density  $\rho_d$  to water content  $w$ , were measured for both soils  
151 according to the procedure proposed by Sivakumar (1993), Sharma (1998) and Raveendiraraj (2009).  
152 Prior to compaction, the dry material was mixed with the desired amount of water using an electrical  
153 planetary blender for at least 3 minutes. The moist soil was left to equalise inside two plastic bags for  
154 a minimum of 24 hours before being statically compacted (in 10 layers for the Nagen soil and 12  
155 layers for Bouisset soil) inside a 50 mm diameter cylindrical mould with a constant vertical  
156 displacement rate of 1.5 mm/min until achieving a target pressure of 400 kPa. The diameter of each  
157 compacted sample was measured three times at different heights while the height was measured three  
158 times at different angles. The volume of the sample was calculated from the average measurements  
159 of diameter and height while the mass was recorded by a scale with a resolution of 0.01 grams. The  
160 water content was calculated as the average of three measurements taken on specimens of about 50  
161 grams from the top, middle and bottom of the sample, respectively, according to the norm NF P94-  
162 050 (1995). The measured values of volume, mass, water content and specific gravity were finally  
163 used to calculate the bulk density, dry density, porosity and degree of saturation of the samples.

164 Figure 1 plots the measured values of dry density  $\rho_d$  versus water content  $w$  for both Nagen and  
165 Bouisset soils together with the respective interpolating curves. Inspection of Figure 1 indicates that  
166 the Nagen soil exhibits lower values of the optimum water content and dry density (i.e. 12.75% and  
167 1643 kg/m<sup>3</sup>) than the Bouisset soil (i.e. 15.0% and 1839 kg/m<sup>3</sup>). The optimum of the Nagen soil  
168 corresponds to a degree of saturation of 55%, which is slightly smaller than the values observed in  
169 similar soils, i.e. 65% - 85% (Tatsuoka, 2015). This difference can be explained by the relatively  
170 modest compaction energy applied in this work compared to the standard Proctor (Sharma, 1998).  
171 The same feature is not observed for the Bouisset soil, which exhibits a finer grading and a higher  
172 retention capacity than the Nagen soil.

173 Triaxial samples of 50 mm diameter and 100 mm height were produced by compacting both soils at  
 174 water contents 4% lower than their respective optimum value, thus resulting in a dry density equal to  
 175 92% of the corresponding optimum level. Dry-of-optimum compaction was chosen because it induces  
 176 a double porosity material fabric with a relatively low air-entry value of suction, which facilitates  
 177 unsaturated testing (Delage et al., 1996; Tarantino and De Col, 2008; Monroy et al., 2010; Casini et  
 178 al., 2012).

179 The initial suction was recorded inside a triaxial cell, via the axis translation technique, on freshly  
 180 compacted samples under a small mean net stress of 20 KPa and restrained pore water drainage. After  
 181 ramping up the cell and pore air pressures to 950 kPa and 930 kPa, respectively, the pore water  
 182 pressure was measured and subtracted from the corresponding pore air pressure to calculate the soil  
 183 suction. Table 3 summarises the average “as-compacted” properties of the triaxial samples of both  
 184 materials.



185

186

Figure 1. Static compaction curves of Nagen and Bouisset soils

**Table 3. Properties of triaxial samples after compaction**

	Water content, $w$ (%)	Bulk density, $\rho_b$ (kg/m <sup>3</sup> )	Dry density, $\rho_d$ (kg/m <sup>3</sup> )	Porosity, $n$ (-)	Void ratio, $e$ (-)	Degree of saturation, $S_r$ (%)	Suction, $s$ (kPa)
NAGEN	8.75	1648	1515	0.430	0.756	30.8	380
BOUISSET	11.0	1884	1698	0.359	0.561	52.1	200

187 ***Triaxial testing equipment***

188 Unsaturated tests were performed by using two identical double-walled triaxial cells commercialised  
189 by the company VJ Tech. The volumetric deformation of the samples was measured by a volume  
190 change device, which was hydraulically connected to the inner cell. Suction was controlled (or  
191 measured) via the axis translation technique by two pumps imposing (or recording) the pore air and  
192 water pressures, respectively. The top and bottom faces of the sample were hydraulically connected  
193 to the pore water line through two saturated porous ceramic discs characterised by an air entry value  
194 of 1500 kPa. A relatively high air entry value was chosen to minimise pore air diffusion and, therefore,  
195 to avoid the formation of bubbles in the pore water line, which would affect measurements.

196 Each test consisted of a combination of the following stages: a) increase/decrease of mean net stress  
197 at constant suction, b) increase/decrease of suction at constant mean net stress and c) increase of mean  
198 net stress at constant water content with the simultaneous measurement of suction.

199 The mean net stress was increased with a rate of 2 kPa/hour and decreased with a rate of 4 kPa/hour,  
200 while suction was increased and decreased with a rate of 2 kPa/hour. Following Al-Sharrad (2013),  
201 the mean net stress and suction were maintained constant at the end of each test stage, during a “rest”  
202 period, until both the specific volume,  $v = 1 + e$  and the specific water volume,  $v_w = 1 + wG_s$   
203 changed less than 0.001 per day. Test stages involving an increase/decrease of mean net stress or an  
204 increase of suction required rest periods of about 48 hours, during which only small variations of  $v$   
205 and  $v_w$  were observed. Conversely, test stages involving a decrease of suction required significantly

206 longer rest periods of about 6 days, during which much larger variations of  $v$  and  $v_w$  were recorded,  
 207 as discussed later.

208 Saturated tests were performed by using a standard triaxial cell commercialised by the company VJ  
 209 Tech. Samples were preliminarily saturated by flushing water from bottom to top, followed by back-  
 210 pressurisation up to 350 kPa under a low mean effective stress of about 5 kPa. After saturation, the  
 211 mean effective stress was increased by augmenting the cell pressure with a rate of 2 kPa/hour while  
 212 maintaining the pore water pressure at 350 kPa. The pore water pressure was controlled by means of  
 213 an automatic pump, which also served the purpose of recording the change of water content inside  
 214 the sample. Given the saturated state of the soil, the volumetric deformations of the sample were  
 215 directly computed from the recorded changes of water content.

216 Table 4 summarises the stages of all tests performed in this work and indicates whether the  
 217 corresponding results were used for model calibration or validation.

**Table 4. Experimental program**

Material	Test name	Test stages	Used for
NAGEN	SAT-N (saturated)	A-B: Isotropic loading $p-u_w = 3\text{ kPa} \rightarrow 240\text{ kPa}$	Validation
	1N (unsaturated)	A-B: Isotropic loading $p_{\text{net}} = 20\text{ kPa} \rightarrow 680\text{ kPa}$ at constant water content after initial equalisation at $s_0 = 210\text{ kPa}$ B-C: unloading $p_{\text{net}} = 680\text{ kPa} \rightarrow 20\text{ kPa}$ at constant suction $s = 210\text{ kPa}$	Calibration
	2N (unsaturated)	A-B: Isotropic loading $p_{\text{net}} = 20\text{ kPa} \rightarrow 560\text{ kPa}$ at constant water content after initial equalisation at $s_0 = 550\text{ kPa}$ B-C: unloading $p_{\text{net}} = 560\text{ kPa} \rightarrow 20\text{ kPa}$ at constant suction $s = 330\text{ kPa}$	Calibration
	3N (unsaturated)	A-B: Isotropic loading $p_{\text{net}} = 20\text{ kPa} \rightarrow 850\text{ kPa}$ at constant suction $s = 50\text{ kPa}$ B-C: unloading $p_{\text{net}} = 850\text{ kPa} \rightarrow 20\text{ kPa}$ at constant suction $s = 50\text{ kPa}$	Validation
BOUISSET	SAT-B (saturated)	A-B: Isotropic loading $p-u_w = 4\text{ kPa} \rightarrow 240\text{ kPa}$	Validation
	1B (unsaturated)	A-B: Isotropic loading $p_{\text{net}} = 20\text{ kPa} \rightarrow 830\text{ kPa}$ at constant water content after initial equalisation at $s_0 = 220\text{ kPa}$ B-C: unloading $p_{\text{net}} = 830\text{ kPa} \rightarrow 20\text{ kPa}$ at constant suction $s = 55\text{ kPa}$	Calibration
	2B (unsaturated)	A-B: Isotropic loading $p_{\text{net}} = 30\text{ kPa} \rightarrow 790\text{ kPa}$ at constant water content after initial equalisation at $s_0 = 500\text{ kPa}$	Calibration

		B-C: unloading $p_{net} = 790 \text{ kPa} \rightarrow 20 \text{ kPa}$ at constant suction $s = 90 \text{ kPa}$	
	3B (unsaturated)	A-B: Isotropic loading $p_{net} = 20 \text{ kPa} \rightarrow 500 \text{ kPa}$ at constant suction $s = 220 \text{ kPa}$ B-C: wetting $s = 220 \text{ kPa} \rightarrow 5 \text{ kPa}$ at constant mean net stress $p_{net} = 500 \text{ kPa}$ C-D: Isotropic unloading $p_{net} = 500 \text{ kPa} \rightarrow 20 \text{ kPa}$ at constant suction $s = 5 \text{ kPa}$	Validation
	4B (unsaturated)	A-B: Isotropic loading $p_{net} = 20 \text{ kPa} \rightarrow 500 \text{ kPa}$ at constant suction $s = 350 \text{ kPa}$ B-C: wetting $s = 350 \text{ kPa} \rightarrow 5 \text{ kPa}$ at constant mean net stress $p_{net} = 500 \text{ kPa}$ C-D: unloading $p_{net} = 500 \text{ kPa} \rightarrow 150 \text{ kPa}$ at constant suction $s = 5 \text{ kPa}$ D-E: drying $s = 5 \text{ kPa} \rightarrow 100 \text{ kPa}$ at constant mean net stress $p_{net} = 150 \text{ kPa}$	Validation

218 ***CALIBRATION OF RETENTION AND MECHANICAL LAWS***

219 In principle, the above retention and mechanical laws can be calibrated by means of two alternative  
220 strategies. The first strategy consists in a simultaneous optimisation of all parameter values inside  
221 each law via a least square regression of experimental data. The second strategy consists instead in  
222 the interpolation of individual features of material behaviour depending on the physical meaning of  
223 each parameter. Bruno and Gallipoli (2019) adopted a hybrid calibration approach that combined the  
224 former strategy for the retention law with the latter strategy for the mechanical law. In the present  
225 work, instead, the former strategy has been adopted for selecting parameter values inside both  
226 retention and mechanical laws via the interpolation of results from tests on unsaturated samples  
227 subjected to constant water content loading followed by unloading at constant suction. Note that each  
228 constant water content loading path allows the simultaneous exploration of relatively large ranges of  
229 mean net stress and suction, which is particularly advantageous for model calibration.

230 The following sections describe the calibration of both the retention and mechanical laws against the  
231 experimental data for Nagen and Bouisset soils.

232

### 233 *Calibration of retention law*

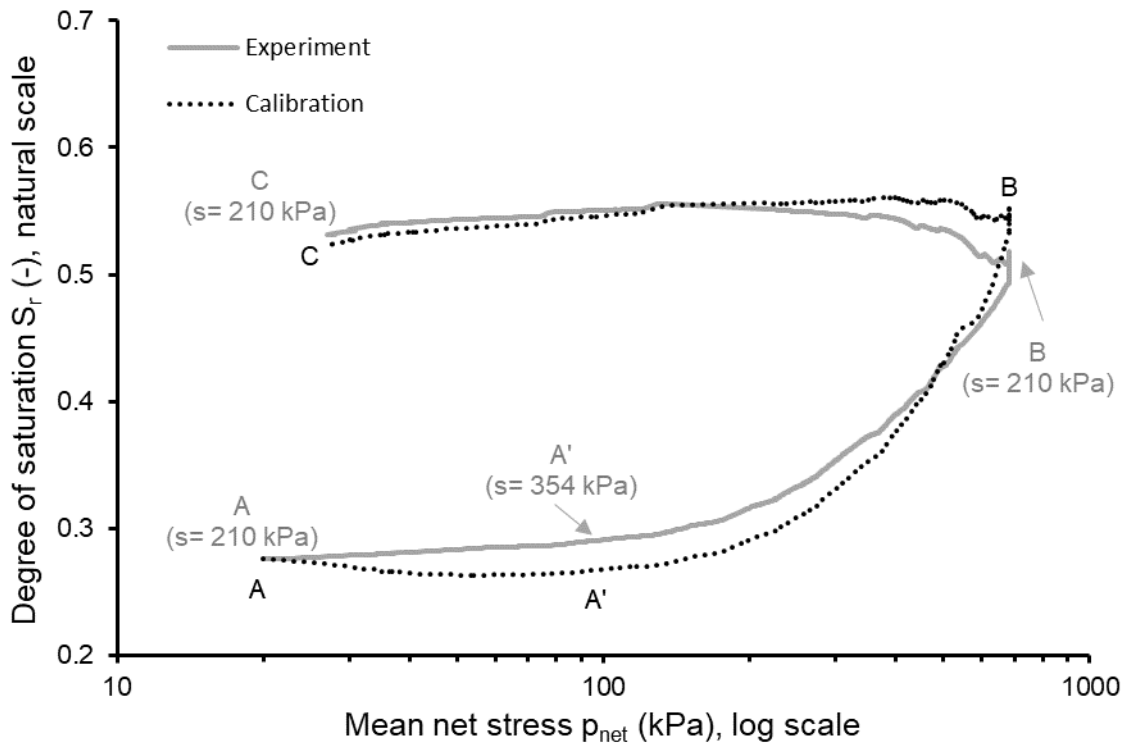
234 The seven parameters (i.e.  $\lambda_s, \omega_w, \beta_w, m_w, \omega_d, \beta_d, m_d$ ) of the retention law were selected, at once, via  
235 a simultaneous least-square regression of two tests for each soil, i.e. tests 1N and 2N for the Nagen  
236 soil and tests 1B and 2B for the Bouisset soil (Table 3). Each of these four tests consisted of a cycle  
237 of mean net stress with loading at constant water content followed by unloading at constant suction.

238 For the Nagen soil, test 1N (Figure 2) involved an initial increase of mean net stress from 20 kPa to  
239 680 kPa at constant water content, followed by a reduction of mean net stress from 680 kPa back to  
240 20 kPa at constant suction of 210 kPa. During the loading stage, suction first increased from 210 kPa  
241 to 354 kPa and then reduced back to 210 kPa. This behaviour is different from that observed during  
242 subsequent tests 2N, 1B and 2B, where suction consistently reduced throughout loading at constant  
243 water content. The difference might have been caused by an accumulation of diffused air into the  
244 pore water line and the consequent formation of air bubbles affecting the measurement of pore water  
245 pressure. Note that test 1N was the first test of the experimental campaign and, for all subsequent  
246 tests, the pore water line was regularly flushed to prevent the potential formation of air bubbles. Test  
247 2N (Figure 3) started with an increase of mean net stress from 20 kPa to 560 kPa at constant water  
248 content, which produced a reduction of suction from 550 kPa to 330 kPa, followed by a reduction of  
249 mean net stress from 560 kPa back to 20 kPa at constant suction of 330 kPa.

250 For the Bouisset soil, test 1B (Figure 4) started with an increase of mean net stress from 20 kPa to  
251 830 kPa at constant water content, which produced a reduction of suction from the initial value of  
252 220 kPa to 55 kPa, followed by a reduction of mean net stress from 830 kPa back to 20 kPa under a  
253 constant suction of 55 kPa. Test 2B (Figure 5) started instead with an increase of mean net stress from  
254 30 kPa to 790 kPa at constant water content, which produced a suction drop from the initial value of  
255 500 kPa to 90 kPa, followed by a reduction of mean net stress from 790 kPa back to 20 kPa at a  
256 constant suction of 90 kPa.

257 Figures 2 to 5 compare the experimental and calibrated variations of degree of saturation for tests 1N,  
258 2N, 1B and 2B. The grey and black labels, placed next to the measured and computed curves  
259 respectively, identify the start and end points of each test stage. The calibrated data were computed  
260 by using either the wetting or drying equation of Table 1 depending on the sign of the variation of the  
261 scaled suction  $\bar{s} = se^{\frac{1}{\lambda_s}}$  defined by Gallipoli et al. (2015). A reduction of scaled suction corresponds  
262 to a wetting path (i.e. increase of degree of saturation) while an increase of scaled suction corresponds  
263 to a drying path (i.e. decrease of degree of saturation). As customary during calibration, experimental,  
264 rather than computed, values of suction and void ratio were used for calculating the scaled suction.  
265 This ensured that the calibrated curves are entirely the product of the retention law with no influence  
266 of the mechanical law. Note that the value of scaled suction varies during both loading at constant  
267 water content and unloading at constant suction as it depends on both suction and void ratio.

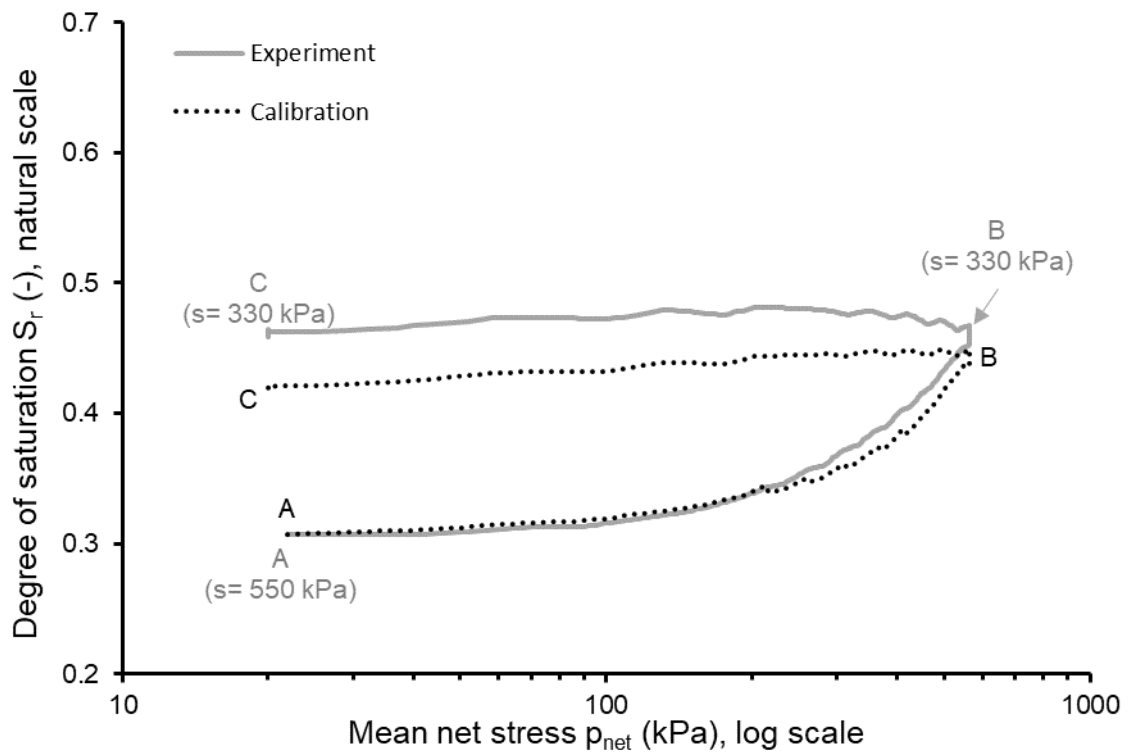
268 The constant of integration  $C_w$  of the first wetting path was calculated by matching the experimental  
269 and calibrated curves at the start of the test to avoid that a poor prediction of the initial state of the  
270 soil would compromise the quality of calibration. Instead, the constant of integration  $C_d$  of the  
271 subsequent drying path was calculated by imposing the continuity of predictions at the reversal point  
272 of the cycle. In general, Figure 2 to 5 show a good agreement between experimental and calibrated  
273 values of degree of saturation, which confirms the ability of the chosen material parameters to capture  
274 the retention behaviour of both Nagen and Bouisset soils. During constant water content loading in  
275 test 1N (Figure 2), the model predicts a slight decrease of degree of saturation from 0.28 (Point A) to  
276 0.26 (Point A') followed by a substantial increase to 0.55 (Point B) whereas the experiment indicates  
277 a monotonic increase of degree of saturation. As discussed earlier, this small discrepancy is caused  
278 by the unrealistic measurement of an increase of suction at the start of loading, probably produced by  
279 the formation of air bubbles in the pore water line. This suction increase is interpreted by the model  
280 as drying, which produces the irregular prediction of degree of saturation during loading.



281

282

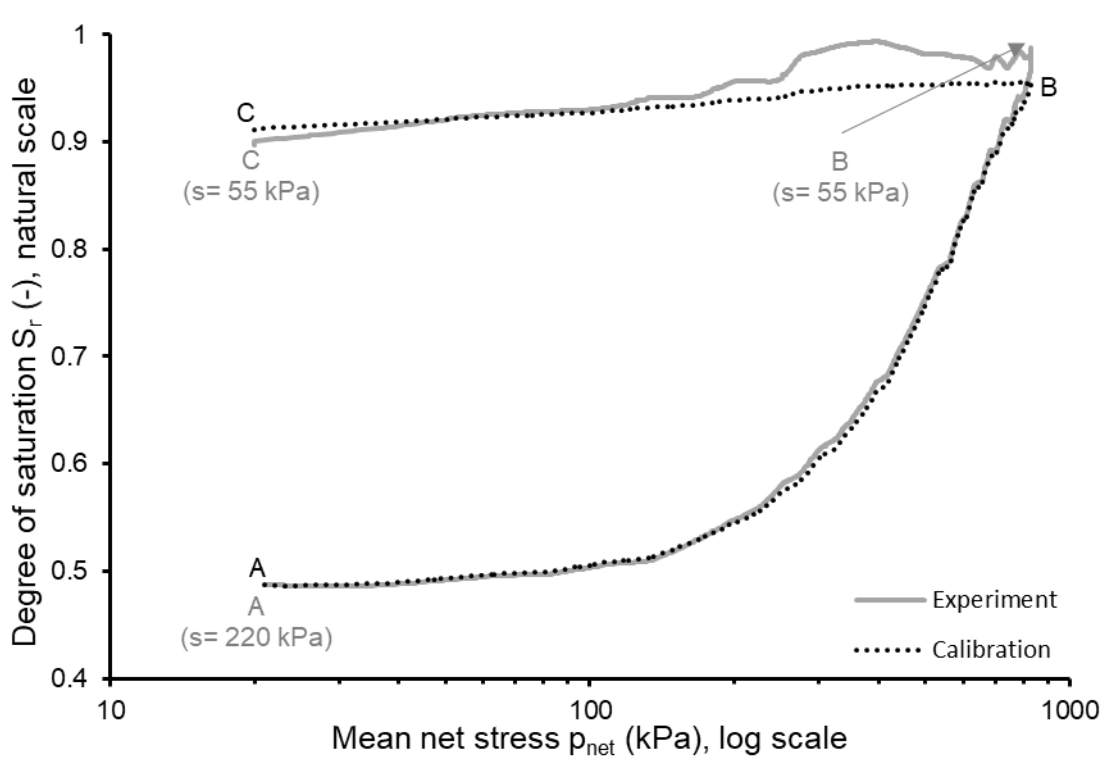
Figure 2. Calibration of retention law against test 1N



283

284

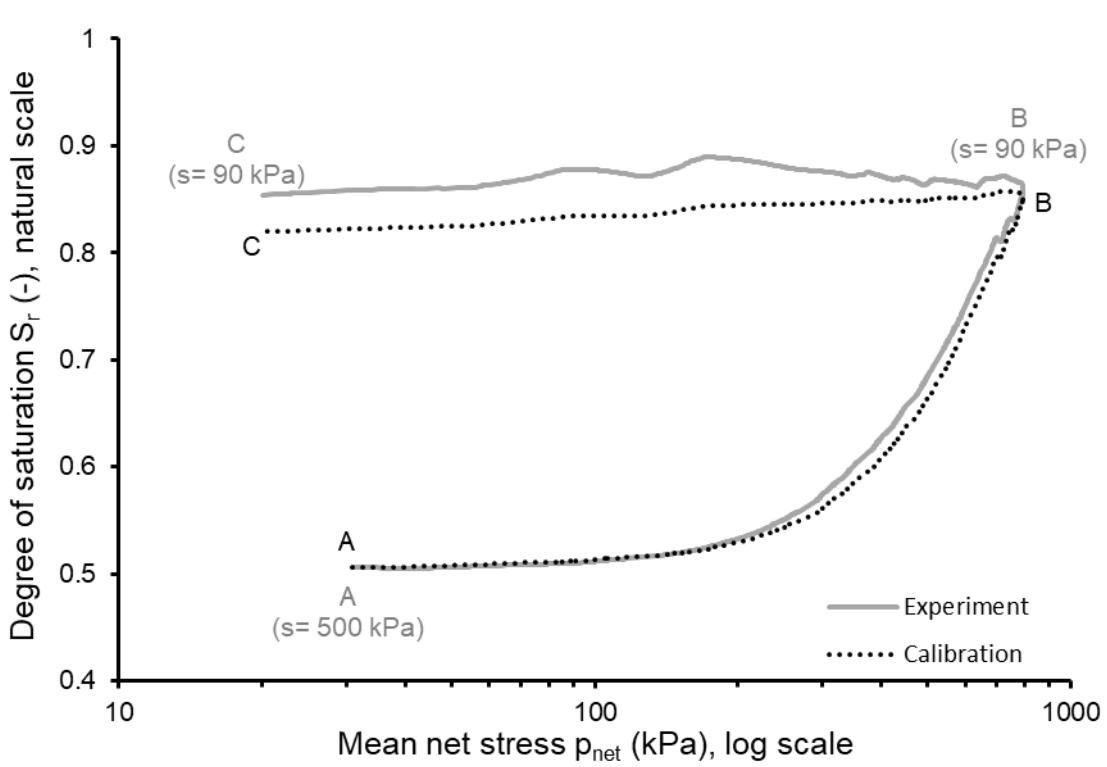
Figure 3. Calibration of retention law against test 2N



285

286

Figure 4. Calibration of retention law against test 1B



287

288

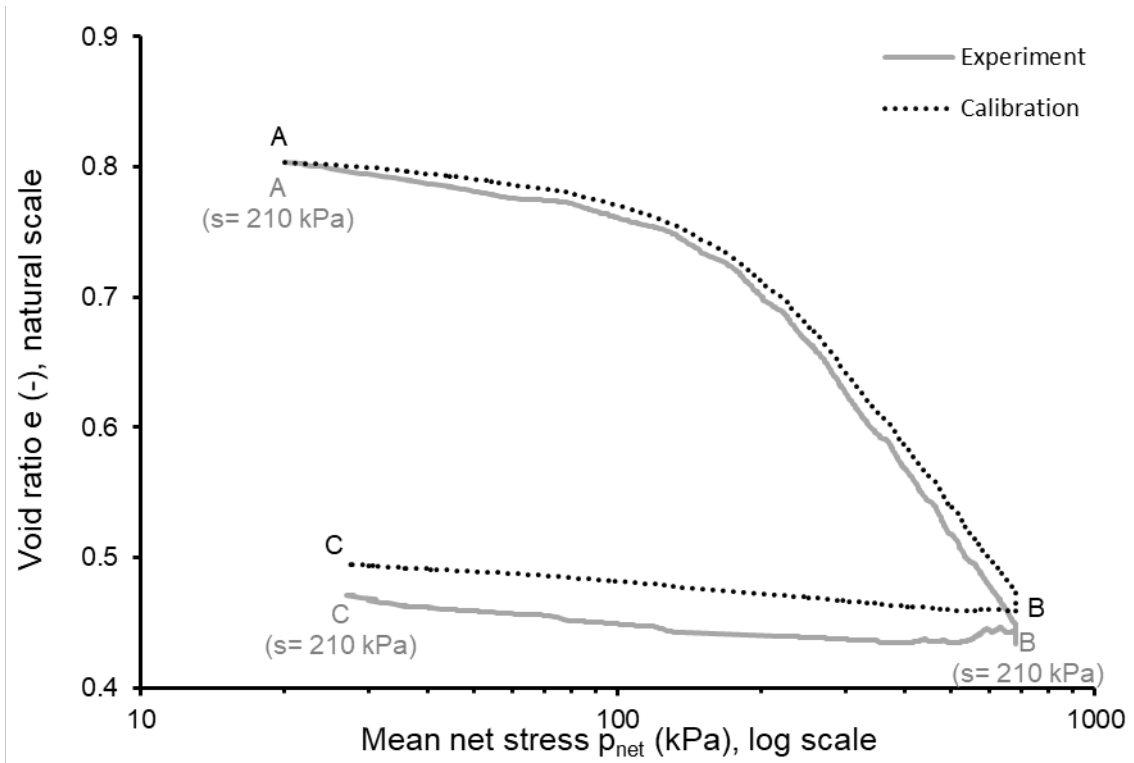
Figure 5. Calibration of retention law against test 2B

289 ***Calibration of mechanical law***

290 The five mechanical parameters (i.e.  $\lambda_p, \bar{p}_{ref}, \lambda_r, k$  and  $\gamma$ ) were selected at once via a least-square  
291 regression of the same four tests used for calibrating the retention law, i.e. tests 1N and 2N for the  
292 Nagen soil (Figures 6 and 7) and tests 1B and 2B for the Bouisset soil (Figures 8 and 9).

293 The calibrated curves were computed by using either the loading or unloading equation of Table 1  
294 depending on the sign of the variation of the mean scaled stress  $\bar{p} = p' S_r^{\frac{\lambda_r}{\lambda_p}}$  defined by Gallipoli and  
295 Bruno (2017). An increase of mean scaled stress corresponds to a loading path (i.e. decrease of void  
296 ratio) while a decrease of mean scaled stress corresponds to an unloading path (i.e. increase of void  
297 ratio). Experimental, rather than computed, values of degree of saturation were considered for  
298 calculating the mean scaled stress, which ensured that the calibrated curves are entirely the product  
299 of the mechanical law with no influence of the retention law.

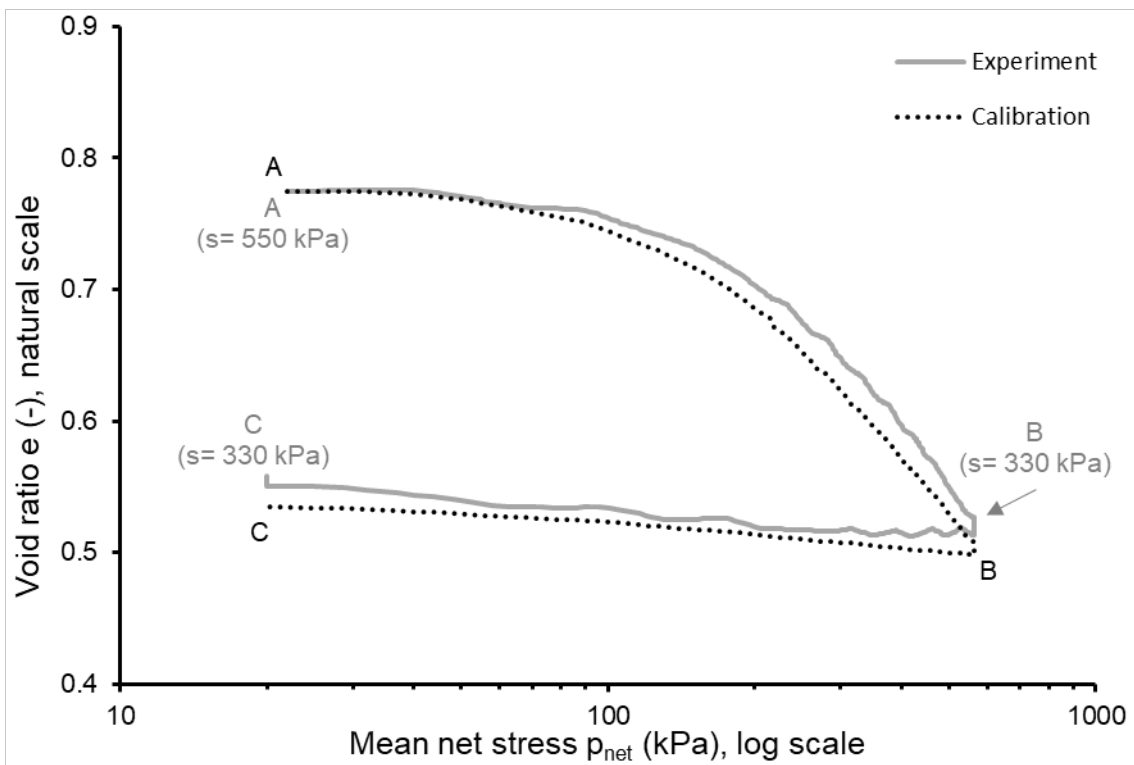
300 Like the retention law, the constant of integration  $C_l$  of the first loading path was calculated by  
301 matching measured and calibrated curves at the start of the test while the constant of integration  $C_u$   
302 of the subsequent unloading path was calculated by imposing the continuity of the predictions at the  
303 reversal point of the cycle. Inspection of Figures 6 to 9 confirms that the calibrated curves accurately  
304 reproduce the mechanical behaviour of both soils, thus confirming the suitability of the chosen  
305 parameter values. The selected parameter values for both the retention and mechanical laws are  
306 summarised in Table 5.



307

308

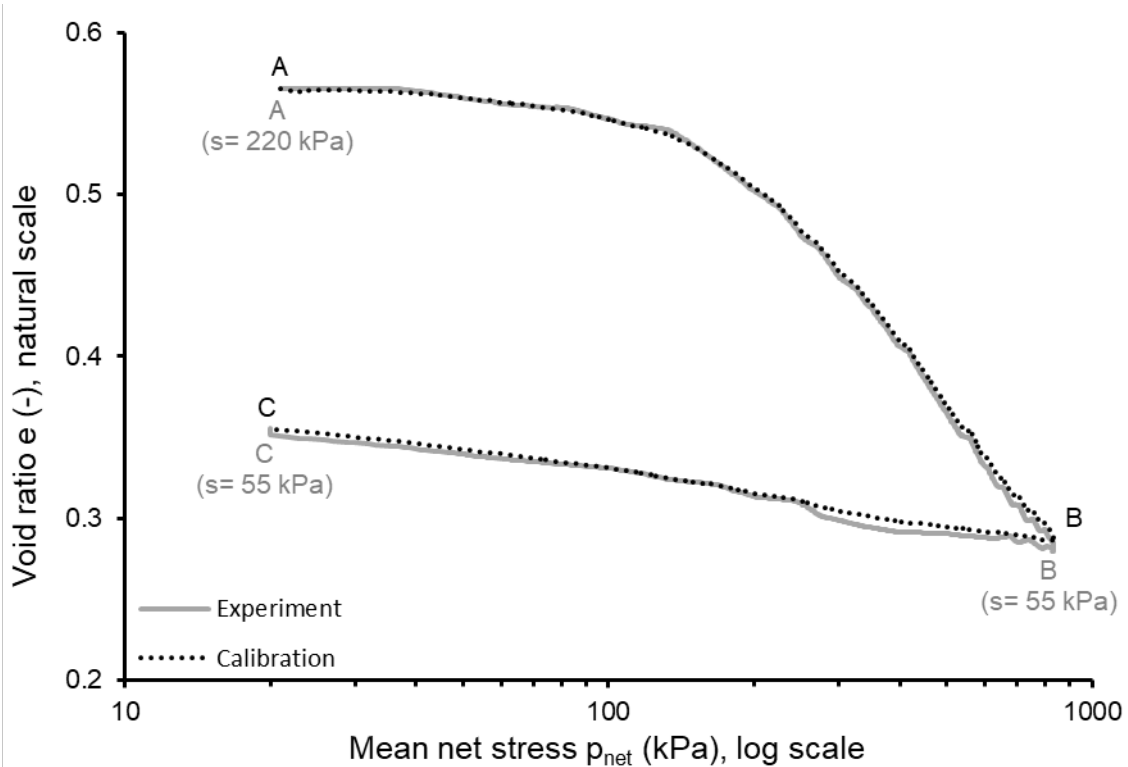
Figure 6. Calibration of mechanical law against test 1N



309

310

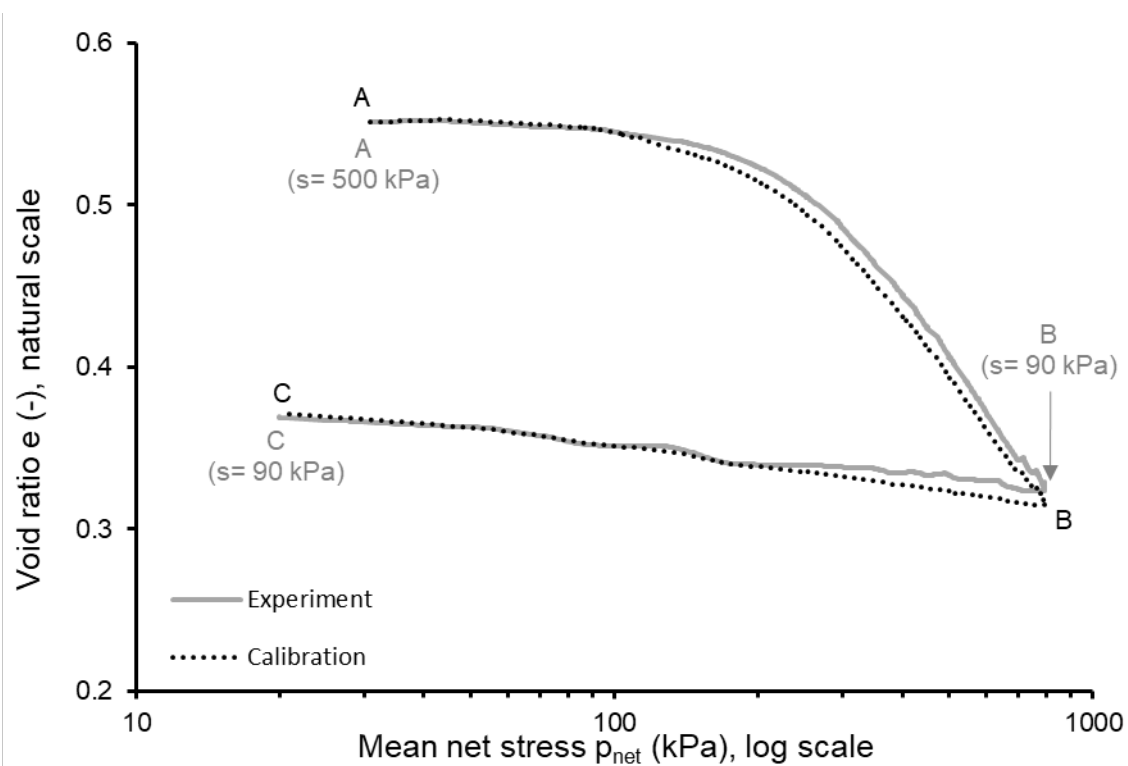
Figure 7. Calibration of mechanical law against test 2N



311

312

Figure 8. Calibration of mechanical law against test 1B



313

314

Figure 9. Calibration of mechanical law against test 2B

315

**Table 5. Values of model parameters**

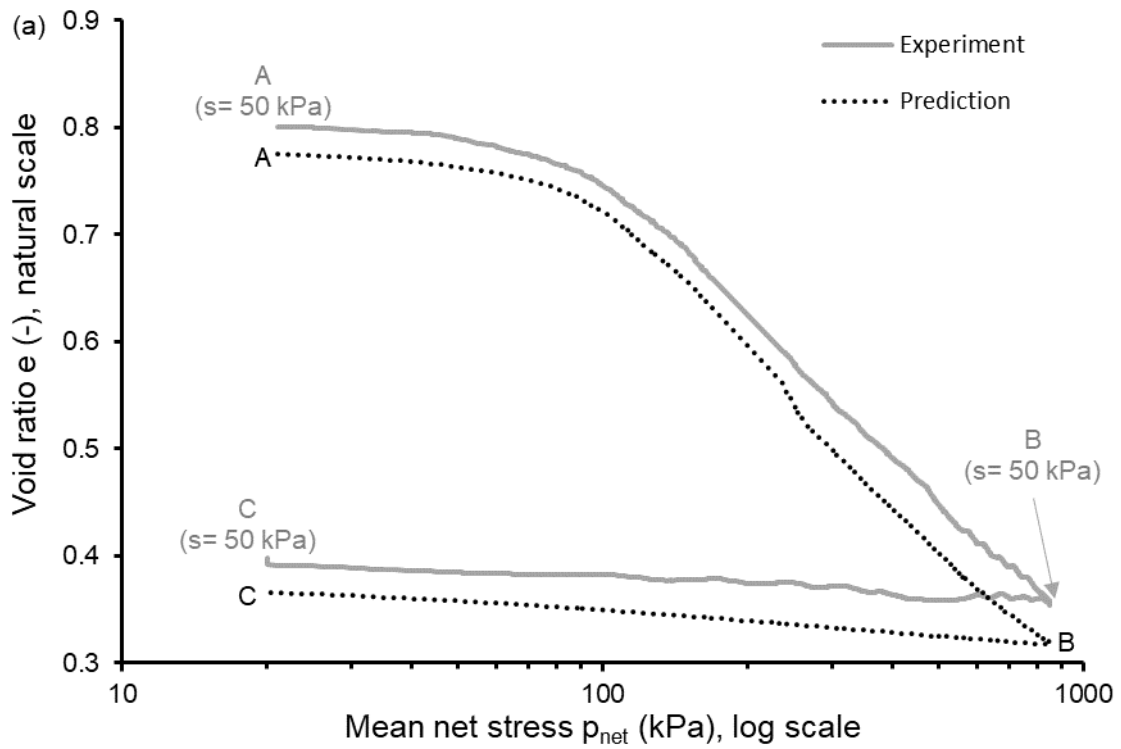
		NAGEN	BOUISSET
Retention parameters	$\lambda_s$	0.214	0.088
	$\omega_w$	0.275 kPa	$3.58 \times 10^{-5}$ kPa
	$m_w$	0.038	0.062
	$\beta_w$	0.608	0.206
	$\omega_d$	26598 kPa	41633 kPa
	$m_d$	0.038	0.062
	$\beta_d$	0.010	0.035
Mechanical parameters	$\lambda_r$	0.539	0.728
	$\lambda_p$	0.220	0.164
	$\bar{p}_{ref}$	4.72 kPa	0.410 kPa
	$\gamma$	2.05	1.23
	$\kappa$	0.050	0.075

316 **VALIDATION OF COUPLED HYDROMECHANICAL MODEL**

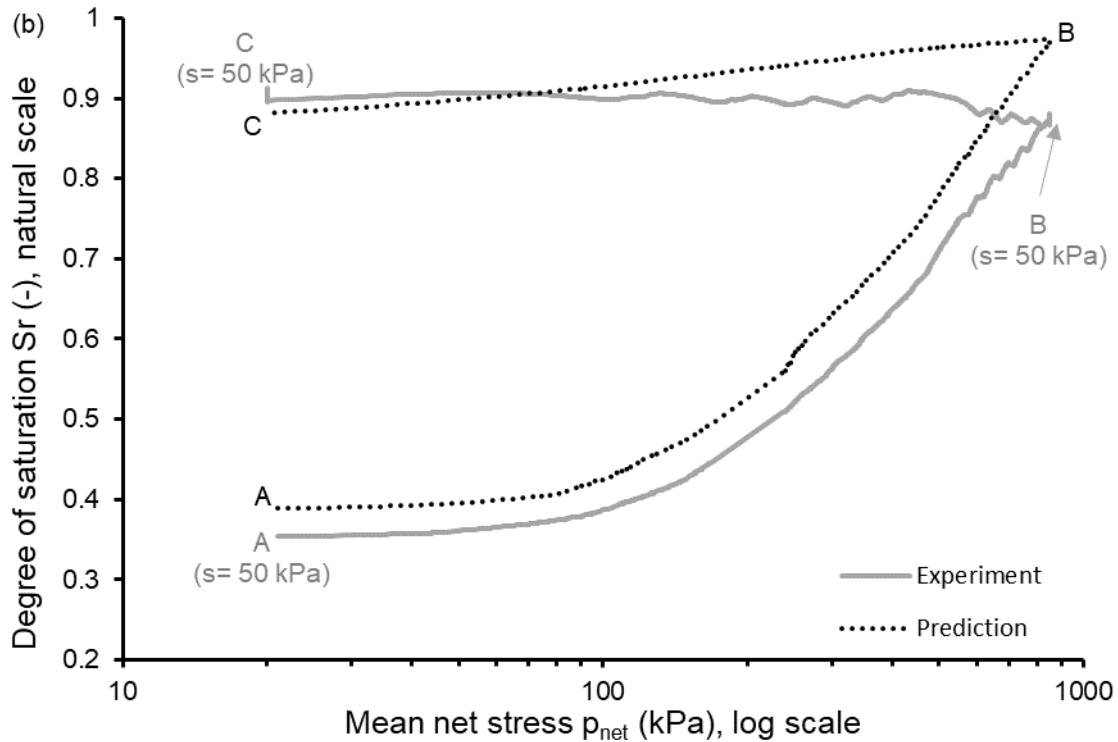
317 The calibrated retention and mechanical laws were coupled via the previously described iterative  
318 algorithm, so that the degree of saturation calculated by the retention law contributes to the  
319 computation of the void ratio by the mechanical law and vice versa. The resulting hydromechanical  
320 model was validated by predicting the degree of saturation and void ratio along stress paths,  
321 formulated in terms of suction and mean net stress, of additional tests not used during previous  
322 calibration.

323 To probe deeper into the model, the initial constants of integration of each test were calculated by  
324 matching predicted and measured data in correspondence of the “as-compacted” soil state (Table 3)  
325 instead of the equalised soil state at the start of the test. Therefore, unlike calibration, the initial  
326 equalised state is now predicted by the model rather than imposed, which also means that the  
327 predicted and experimental curves of each test do not start from the same point. This approach  
328 constitutes a stricter assessment of the model performance, which can no longer rely on the perfect  
329 match between predictions and experiments at the start of the test.

330 For the Nagen soil, model predictions were validated against results from test 3N (Table 4), which  
331 consists in a cycle of mean net stress from 20 kPa to 850 kPa and back to 20 kPa at a constant suction  
332 of 50 kPa. Figures 10 shows a generally good agreement between the experimental and predicted  
333 curves of both void ratio and degree of saturation. Note also that Test 3N was performed at a constant  
334 suction of 50 kPa, which is lower than the suction range explored during calibration. This result,  
335 therefore, indicates the ability of the model to extrapolate predictions beyond the original  
336 experimental data.



337



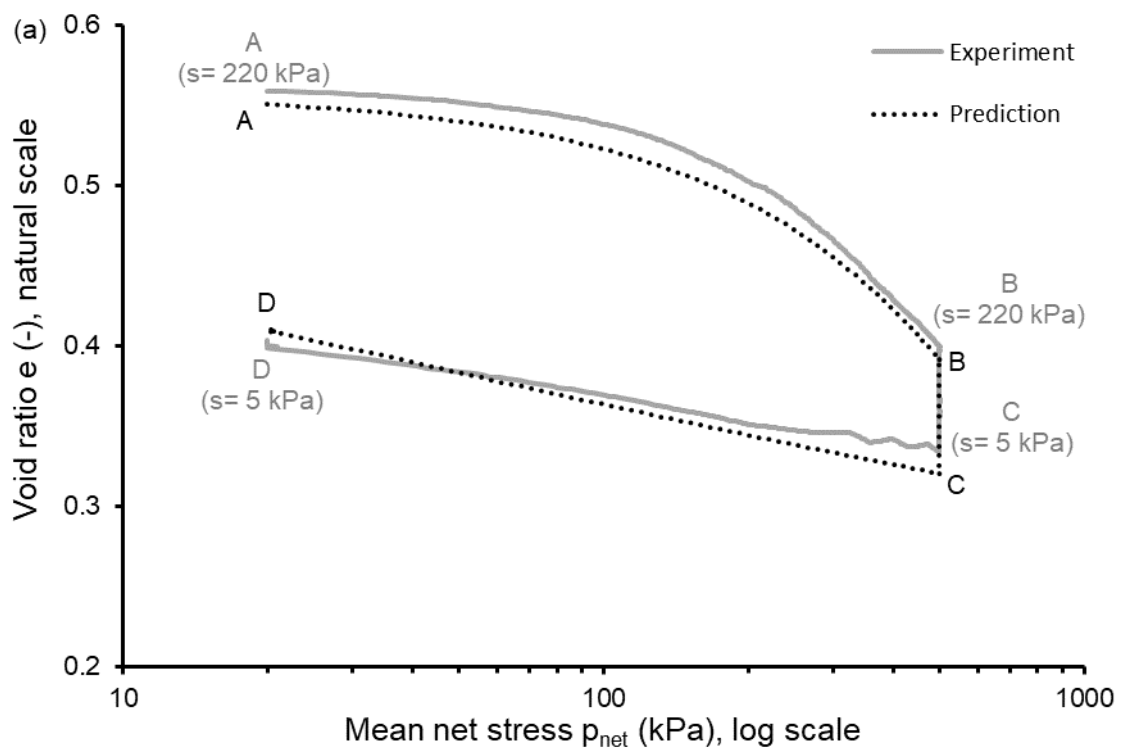
338

339 *Figure 10. Model validation against test 3N: (a) void ratio vs mean net stress and (b) degree of*  
 340 *saturation vs mean net stress*

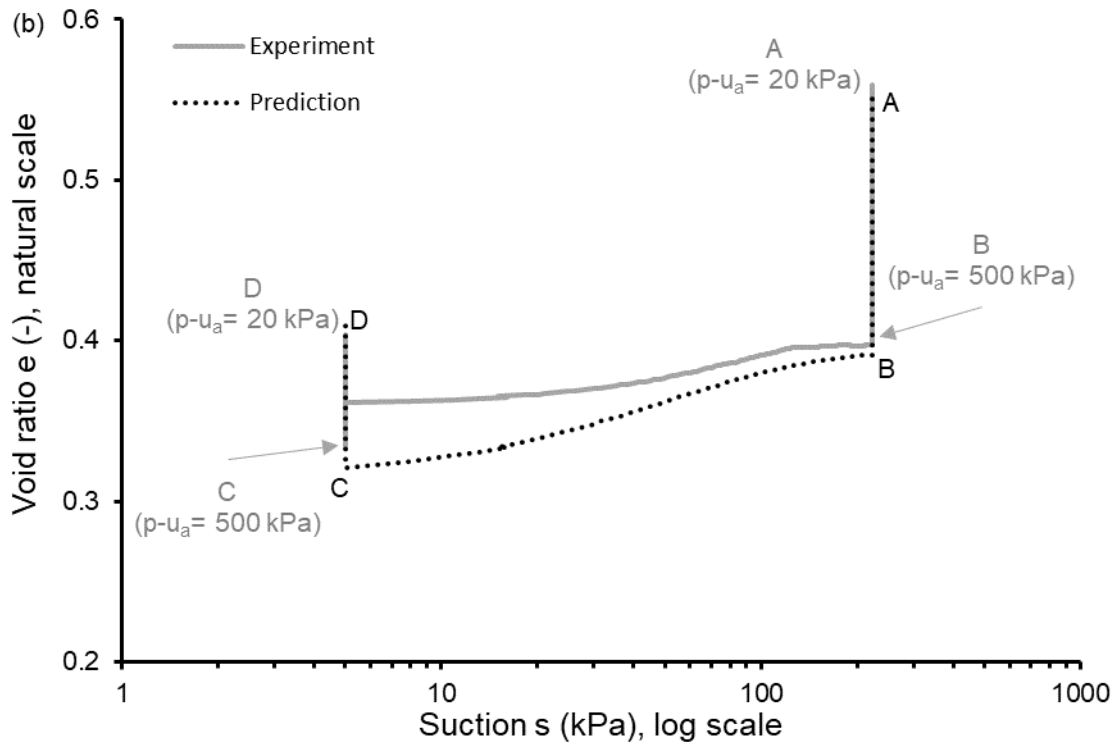
341 For the Bouisset soil, model predictions were validated against two tests, i.e. 3B and 4B, which  
 342 involved cyclic variations of mean net stress and suction (Table 4). Both tests start with an increase  
 343 of mean net stress from 20 kPa to 500 kPa at constant suction of 220 kPa, for test 3B, and 350 kPa,  
 344 for test 4B. Suction is then decreased to 5 kPa in both tests at a constant mean net stress of 500 kPa,  
 345 followed by a reduction of mean net stress to 20 kPa, for test 3B, and 150 kPa, for test 4B, at a constant  
 346 suction of 5 kPa. Finally, test 4B undergoes an increase of suction from 5 kPa to 100 kPa at a constant  
 347 mean net stress of 150 kPa.

348 Figures 11 and 12 show generally good predictions of degree of saturation and void ratio under  
 349 varying levels of mean net stress and suction, including a relatively accurate prediction of degree of  
 350 saturation and volumetric collapse after the rest periods at the end of the suction reduction stages (i.e.  
 351 stages BC). The discrepancies between experiments and predictions along wetting paths are mostly

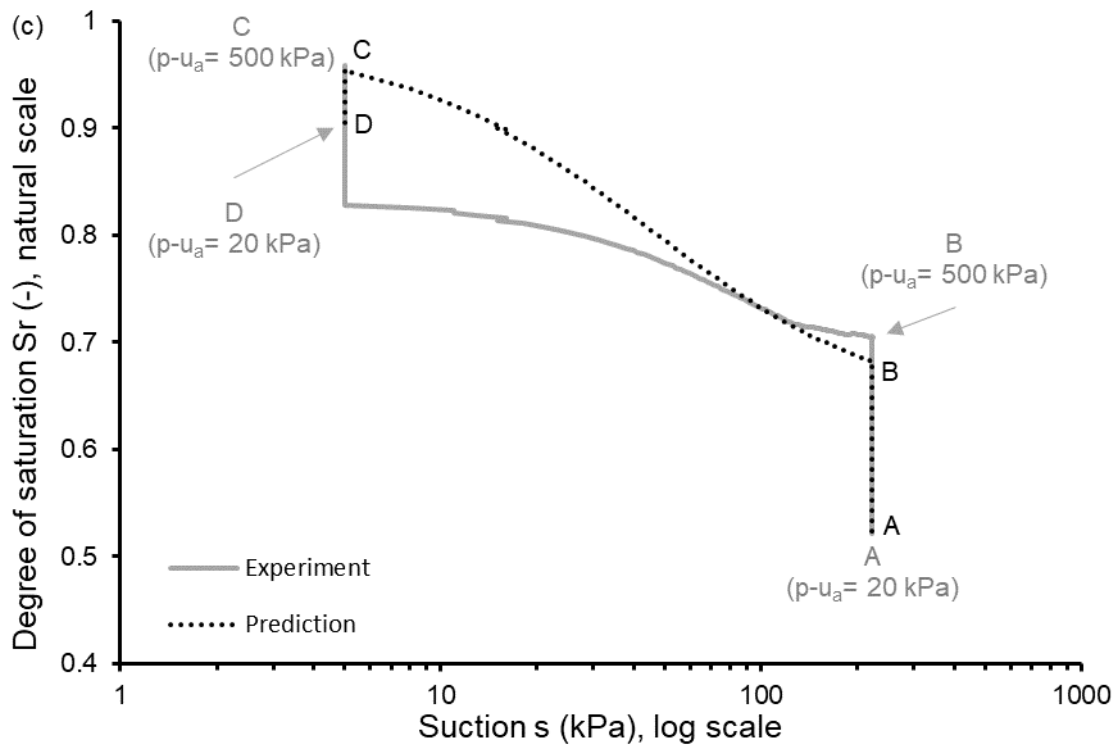
352 due to the relatively high suction reduction rate (2 kPa/hour) during experiments, which was too fast  
 353 to allow the equalisation of pore water pressure inside the sample. This is confirmed by the significant  
 354 increase of degree of saturation, and the associated decrease of void ratio, during the rest periods at  
 355 the end of the suction reduction stages. With the benefit of hindsight, a slower suction reduction rate  
 356 should have been imposed or, at least, suction should have been measured at the sample mid-height  
 357 by means of high capacity tensiometers to cross-check equalisation inside the soil. Note that the  
 358 wetting-induced collapse of compacted/reconstituted samples may not be fully representative of the  
 359 behaviour of undisturbed collapsible soils. This aspect is, however, outside the scope of the present  
 360 paper and will constitute matter for future research.



361



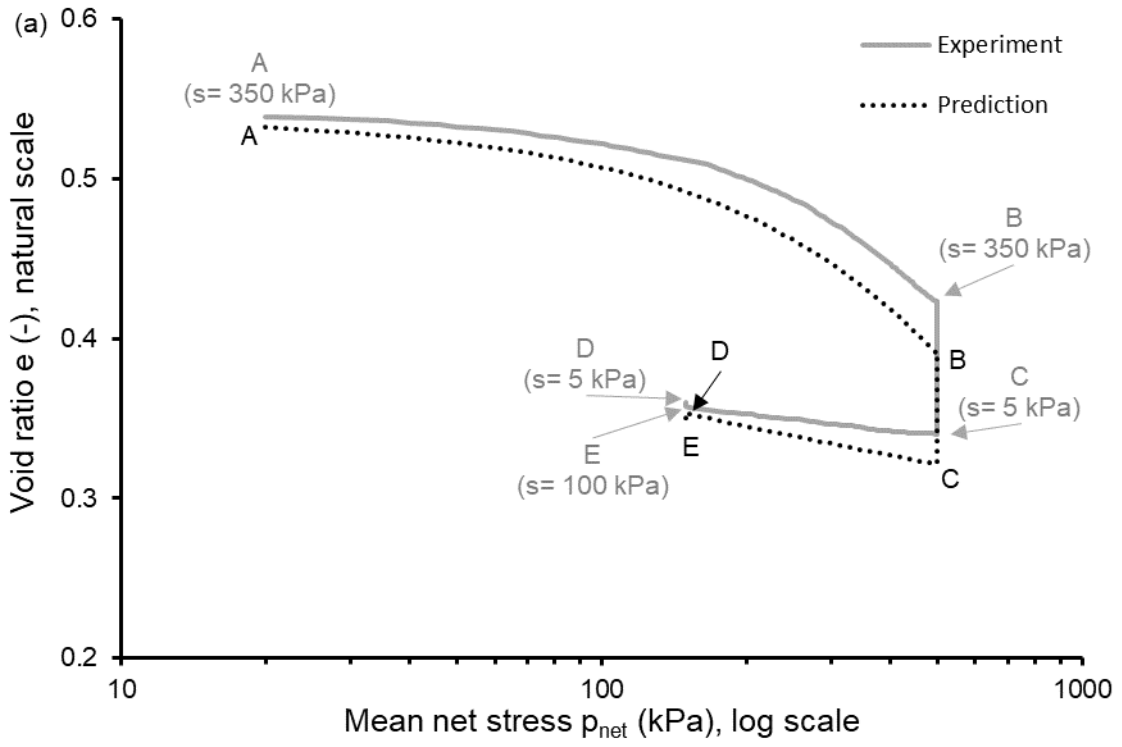
362



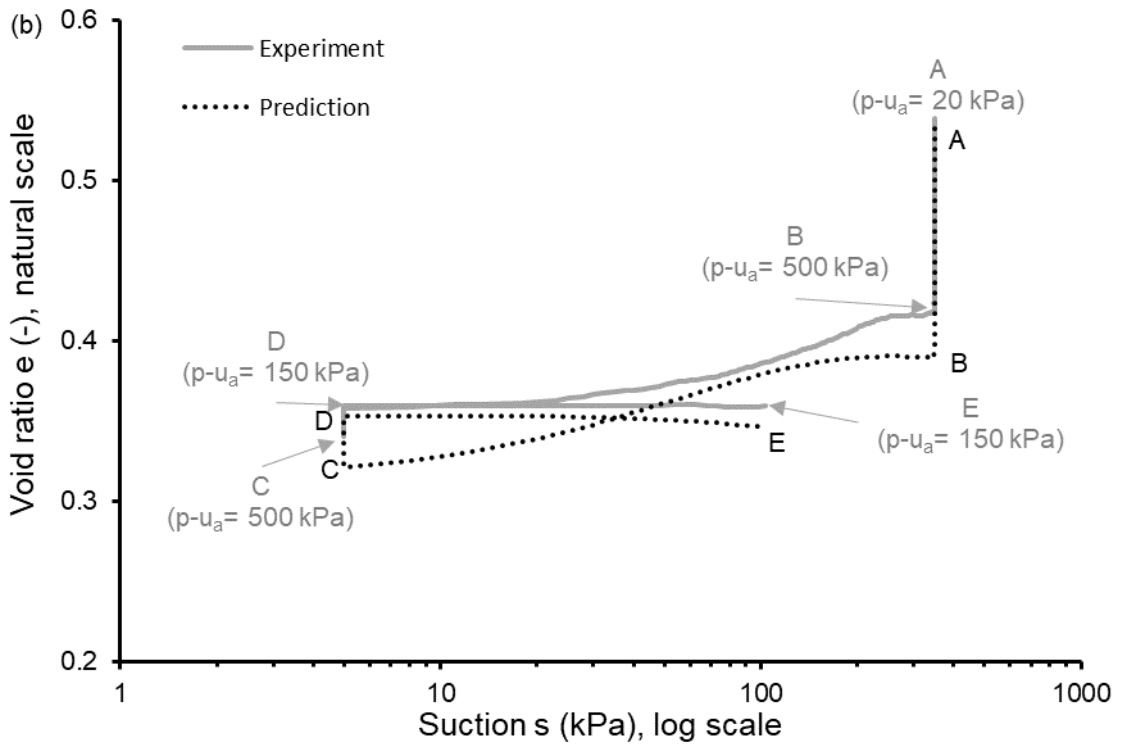
363

364 *Figure 11. Model validation against test 3B: (a) void ratio vs mean net stress, (b) void ratio vs*

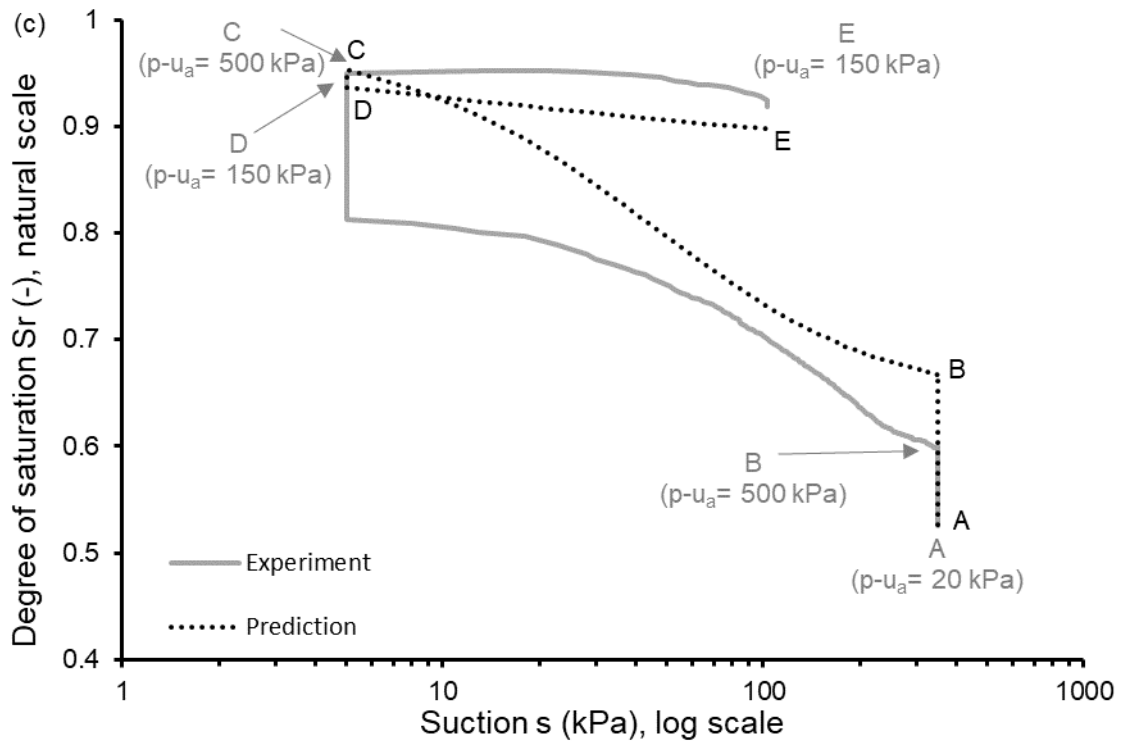
365 *suction and (c) degree of saturation vs suction*



366



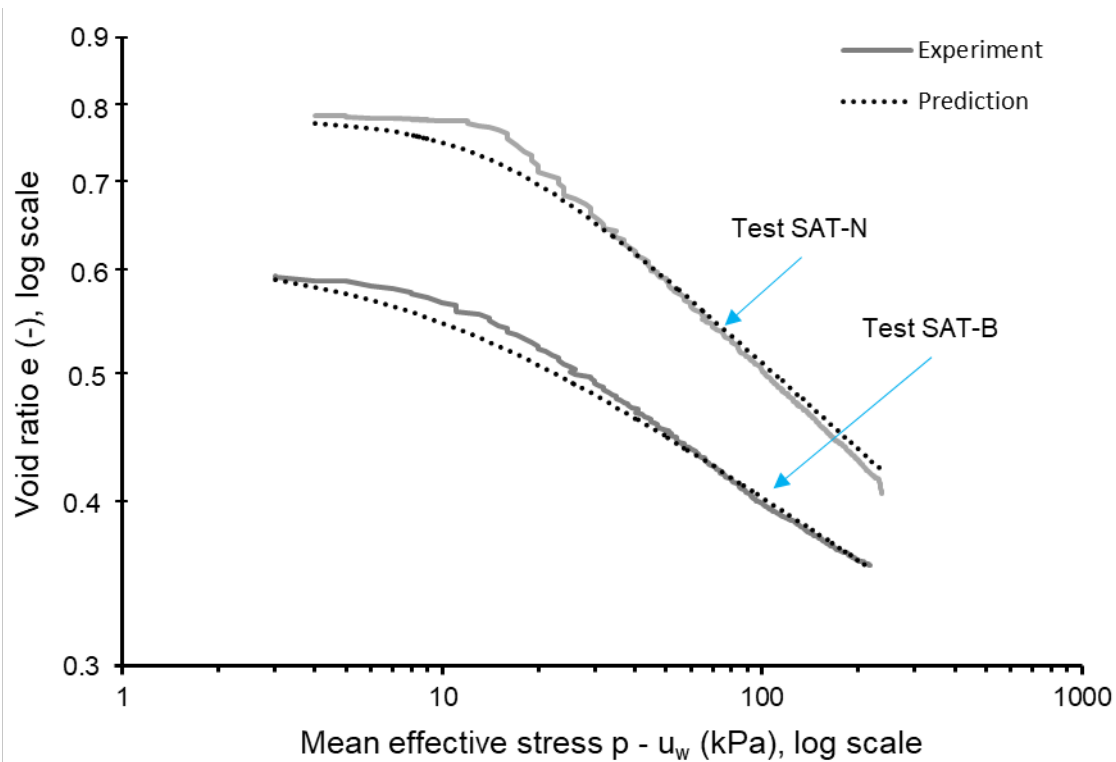
367



368

369 *Figure 12. Model validation against test 4B: (a) void ratio vs mean net stress, (b) void ratio vs*  
 370 *suction and (c) degree of saturation vs suction*

371 Figure 13 shows the results from two saturated tests, i.e. test SAT-N on Nagen soil and test SAT-B  
 372 on Bouisset soil (Table 4), together with the corresponding model prediction. Note that the soil state  
 373 at the start of both tests was predicted by the model via the simulation of the initial saturation of the  
 374 sample under a low confining pressure of about 5 kPa. Inspection of Figure 13 indicates that, in both  
 375 cases, the model successfully predict the full saturation and swelling of the sample as suction changes  
 376 from the value after compaction to zero. Importantly, the same model parameters determined from  
 377 unsaturated tests (i.e. tests 1N and 2N for Nagen soil or tests 1B and 2B for Bouisset soil - see section  
 378 on mechanical calibration) provide an excellent match also to the two saturated tests. This confirms  
 379 the ability of the model to predict soil deformations regardless of the saturation state of the soil, which  
 380 corroborates the unifying modelling approach of Gallipoli and Bruno (2017).



381

382 *Figure 13. Model validation against the saturated tests SAT-N and SAT-B performed on Nagen and*  
 383 *Bouisset soil, respectively.*

384 **CONCLUSIONS**

385 This paper has presented original data from a series of unsaturated and saturated isotropic tests  
 386 performed on compacted samples of a sandy silt (Nagen soil) and a clayey silt (Bouisset soil) inside  
 387 triaxial cells. The tests involved either an increase/decrease of mean net stress at constant suction or  
 388 an increase-decrease of suction at constant mean net stress. Some samples were also subjected to an  
 389 increase of mean net stress at constant water content with the simultaneous measurement of suction.  
 390 During all tests, the void ratio and the degree of saturation were continuously recorded to assess the  
 391 mechanical and retention behaviour of the soils. Test results were subsequently used for the  
 392 calibration and validation of the bounding surface hysteretic hydromechanical model of Bruno and  
 393 Gallipoli (2019). The main findings can be summarised as follows:

- 394 • Loading at constant water content with measurement of suction is highly convenient for model  
395 calibration as it allows the simultaneous exploration of relatively large ranges of mean net and  
396 suction via a limited number of fast tests.
- 397 • The model reproduces well the unsaturated hydromechanical behaviour of both the sandy silt  
398 and clayey silt tested in this work. This result also extends the previous validation of the  
399 model, which was limited to finer soils from bentonitic and kaolinitic clays to loess silts.
- 400 • The progressive yielding and smooth retention response of the soils are well captured by the  
401 adopted bounding surface model.
- 402 • The model correctly predicts the magnitude of volumetric collapse and saturation during  
403 wetting at constant mean net stress, though some discrepancies exist due to the relatively high  
404 rate of suction reduction imposed during the tests.
- 405 • The saturated behaviour of the two soils is accurately reproduced by the model using the  
406 parameters selected by fitting only unsaturated tests. This corroborates the efficacy of the  
407 scaled constitutive variables in unifying the behaviour of saturated and unsaturated soils  
408 within a single material framework.

409 Future work will focus on extending the validation of the hydromechanical model to  
410 intact/undisturbed soils.

## 411 ***REFERENCES***

- 412 AFNOR (1991). NF P 94-054; Soils: investigation and testing – Determination of particle density-  
413 Pycnometer method.
- 414 AFNOR (1992). NF P 94-057. Soils: investigation and testing – Granulometric analysis – Hydrometer  
415 method.
- 416 AFNOR (1993). NF P 94-051; Soils: Investigation and testing – Determination of Atterberg’s limits  
417 – Liquid limit test using Casagrande apparatus – Plastic limit test on rolled thread.
- 418 AFNOR (1995). NF P94-050. Soils: investigation and testing. Determination of moisture content.  
419 Oven drying method.

420 AFNOR (1995). XP P 94-041. Soils: investigation and testing – Granulometric description – Wet  
421 sieving method.

422 Al-Sharrad, M. A. (2013). *Evolving anisotropy in unsaturated soils: experimental investigation and*  
423 *constitutive modelling* (Doctoral dissertation, University of Glasgow).

424 Alonso, E. E., Gens, A., & Josa, A. (1990). A constitutive model for partially saturated soils.  
425 *Géotechnique*, 40(3), 405-430.

426 Balzano, B., Bruno, A. W., Denzer, H., Molan, D., Tarantino, A., & Gallipoli, D. (2021). REAL-  
427 TIME quality check of measurements of soil water status in the vadose zone. *Physics and Chemistry*  
428 *of the Earth, Parts A/B/C*, 121, 102918.

429 Bruno, A. W., & Gallipoli, D. (2019). A coupled hydromechanical bounding surface model predicting  
430 the hysteretic behaviour of unsaturated soils. *Computers and Geotechnics*, 110, 287-295.

431 Bruno, A. W., Gallipoli, D., Perlot, C., & Mendes, J. (2017). Mechanical behaviour of  
432 hypercompacted earth for building construction. *Materials and Structures*, 50(2), 1-15.

433 Casini, F., Vaunat, J., Romero, E., & Desideri, A. (2012). Consequences on water retention properties  
434 of double-porosity features in a compacted silt. *Acta Geotechnica*, 7(2), 139-150.

435 Cuccurullo, A., Gallipoli, D., Bruno, A. W., Augarde, C. E., Hughes, P., & La Borderie, C. (2018,  
436 January). Influence of Soil Grading on the Hygro-Mechanical Properties of Hyper-Compacted Earth  
437 for Masonry Construction. In *10th International Masonry Conference (10thIMC)* (pp. 1459-1471).

438 Cunningham, M. R., Ridley, A. M., Dineen, K., & Burland, J. B. (2003). The mechanical behaviour  
439 of a reconstituted unsaturated silty clay. *Géotechnique*, 53(2), 183-194.

440 Delage, P., Audiguier, M., Cui, Y. J., & Howat, M. D. (1996). Microstructure of a compacted  
441 silt. *Canadian Geotechnical Journal*, 33(1), 150-158.

442 Delage, P., Howat, M. D., & Cui, Y. J. (1998). The relationship between suction and swelling  
443 properties in a heavily compacted unsaturated clay. *Engineering geology*, 50(1-2), 31-48.

444 Fredlund, D. G., & Wong, D. K. (1989). Calibration of thermal conductivity sensors for measuring  
445 soil suction. *Geotechnical Testing Journal*, 12(3), 188-194.

446 Fredlund, D. G., & Xing, A. (1994). Equations for the soil-water characteristic curve. *Canadian*  
447 *geotechnical journal*, 31(4), 521-532.

448 Gallipoli, D., Bruno, A. W., D’Onza, F., & Mancuso, C. (2015). A bounding surface hysteretic water  
449 retention model for deformable soils. *Géotechnique*, 65(10), 793-804.

450 Gallipoli, D., & Bruno, A. W. (2017). A bounding surface compression model with a unified virgin  
451 line for saturated and unsaturated soils. *Géotechnique*, 67(8), 703-712.

452 Gallipoli, D., Gens, A., Sharma, R., & Vaunat, J. (2003b). An elasto-plastic model for unsaturated  
453 soil incorporating the effects of suction and degree of saturation on mechanical behaviour.  
454 *Géotechnique*, 53(1), 123-136.

- 455 Gallipoli, D., Wheeler, S. J., & Karstunen, M. (2003a). Modelling the variation of degree of saturation  
456 in a deformable unsaturated soil. *Géotechnique*, 53(1), 105-112.
- 457 Geiser, F., Laloui, L., & Vulliet, L. (2006). Elasto-plasticity of unsaturated soils: laboratory test  
458 results on a remoulded silt. *Soils and Foundations*, 46(5), 545-556.
- 459 Gan, J. K. M., Fredlund, D. G., & Rahardjo, H. (1988). Determination of the shear strength parameters  
460 of an unsaturated soil using the direct shear test. *Canadian Geotechnical Journal*, 25(3), 500-510.
- 461 Jotisankasa, A., Ridley, A., & Coop, M. (2007). Collapse behavior of compacted silty clay in suction-  
462 monitored oedometer apparatus. *Journal of Geotechnical and Geoenvironmental Engineering*,  
463 133(7), 867-877.
- 464 Khalili, N., Habte, M. A., & Zargarbashi, S. (2008). A fully coupled flow deformation model for  
465 cyclic analysis of unsaturated soils including hydraulic and mechanical hystereses. *Computers and*  
466 *Geotechnics*, 35(6), 872-889.
- 467 Lim, B. F., & Siemens, G. A. (2016). Unifying framework for modeling swelling soil behaviour.  
468 *Canadian Geotechnical Journal*, 53(9), 1495-1509.
- 469 Lloret-Cabot, M., Sánchez, M., & Wheeler, S. J. (2013). Formulation of a three-dimensional  
470 constitutive model for unsaturated soils incorporating mechanical–water retention couplings.  
471 *International Journal for Numerical and Analytical Methods in Geomechanics*, 37(17), 3008-3035.
- 472 Lloret-Cabot, M., Wheeler, S. J., Pineda, J. A., Romero, E., & Sheng, D. (2018). From saturated to  
473 unsaturated conditions and vice versa. *Acta Geotechnica*, 13(1), 15-37.
- 474 Lloret-Cabot, M., Wheeler, S. J., & Sánchez, M. (2017). A unified mechanical and retention model  
475 for saturated and unsaturated soil behaviour. *Acta Geotechnica*, 12(1), 1-21.
- 476 Lourenço, S.D.N., Gallipoli, D., Toll, D.G., Augarde, C.E., & Evans, F.D. (2011). A new procedure  
477 for the determination of the soil-water retention curves by continuous drying using high-suction  
478 tensiometers. *Canadian Geotechnical Journal*, 48(2): 327–335
- 479 Lourenço, S.D.N., Gallipoli, D., Toll, D.G., Augarde, C.E., Evans, F.D., & Medero, G.M. (2008).  
480 Calibrations of a high-suction tensiometer. *Géotechnique*, 58(8): 659–668
- 481 Mendes, J., Gallipoli, D., Tarantino, A., & Toll, D. (2019). On the development of an ultra-high-  
482 capacity tensiometer capable of measuring water tensions to 7 MPa. *Géotechnique*, 69(6), 560-564.
- 483 Mendes, J., Toll, D. G., Augarde, C. E., Gallipoli, D., & Wheeler, S. J. (2008). A system for field  
484 measurement of suction using high capacity tensiometers. *Unsaturated Soils: Advances in Geo-*  
485 *Engineering (eds Toll, DG, Augarde, CE, Gallipoli, D. & Wheeler, SJ)*, 219-225.
- 486 Monroy, R., Zdravkovic, L., & Ridley, A. (2010). Evolution of microstructure in compacted London  
487 Clay during wetting and loading. *Géotechnique*, 63(6), 463-478.
- 488 Nuth, M., & Laloui, L. (2008). Advances in modelling hysteretic water retention curve in deformable  
489 soils. *Computers and Geotechnics*, 35(6), 835-844.

- 490 Oka, F., Kodaka, T., Suzuki, H., Kim, Y. S., Nishimatsu, N., & Kimoto, S. (2010). Experimental  
491 study on the behavior of unsaturated compacted silt under triaxial compression. *Soils and foundations*,  
492 50(1), 27-44.
- 493 Raveendraraj, A. (2009). *Coupling of mechanical behaviour and water retention behaviour in*  
494 *unsaturated soils* (Doctoral dissertation, University of Glasgow).
- 495 Ridley, A. M., & Burland, J. B. (1993). A new instrument for the measurement of soil moisture  
496 suction. *Géotechnique*, 43(2), 321-324.
- 497 Romero, E., Della Vecchia, G., & Jommi, C. (2011). An insight into the water retention properties of  
498 compacted clayey soils. *Géotechnique*, 61(4), 313-328.
- 499 Sharma, R. S. (1998). *Mechanical behaviour of unsaturated highly expansive clays* (Doctoral  
500 dissertation, University of Oxford).
- 501 Siemens, G. A., Take, W. A., & Peters, S. B. (2014). Physical and numerical modeling of infiltration  
502 including consideration of the pore-air phase. *Canadian geotechnical journal*, 51(12), 1475-1487.
- 503 Sivakumar, V. (1993). *A critical state framework for unsaturated soil* (Doctoral dissertation,  
504 University of Sheffield).
- 505 Skempton, A. W. (1953). The colloidal activity of clays. *Selected Papers on Soil Mechanics*, 106-  
506 118.
- 507 Sun, D. A., Sheng, D., Xiang, L., & Sloan, S. W. (2008). Elastoplastic prediction of hydro-mechanical  
508 behaviour of unsaturated soils under undrained conditions. *Computers and Geotechnics*, 35(6), 845-  
509 852.
- 510 Sun, D. A., Zhang, J., Gao, Y., & Sheng, D. (2016). Influence of suction history on hydraulic and  
511 stress-strain behavior of unsaturated soils. *International Journal of Geomechanics*, 16(6), D4015001.
- 512 Tarantino, A. (2009). A water retention model for deformable soils. *Géotechnique*, 59(9), 751-762.
- 513 Tarantino, A., & De Col, E. (2008). Compaction behaviour of clay. *Géotechnique*, 58(3), 199-213.
- 514 Tarantino, A., & Tombolato, S. (2005). Coupling of hydraulic and mechanical behaviour in  
515 unsaturated compacted clay. *Géotechnique*, 55(4), 307-317.
- 516 Tatsuoka, F. (2015). Compaction characteristics and physical properties of compacted soil controlled  
517 by the degree of saturation. In *Keynote lecture, deformation characteristics of geomaterials.*  
518 *Proceedings of the 6<sup>th</sup> International Conference on Deformation Characteristics of Geomaterials*,  
519 Buenos Aires (pp. 40-78).
- 520 Tinjum, J. M., Benson, C. H., & Blotz, L. R. (1997). Soil-water characteristic curves for compacted  
521 clays. *Journal of geotechnical and geoenvironmental engineering*, 123(11), 1060-1069.
- 522 Toll, D. G., Lourenço, S. D., & Mendes, J. (2013). Advances in suction measurements using high  
523 suction tensiometers. *Engineering Geology*, 165, 29-37.

- 524 Van Genuchten, M. T. (1980). A closed-form equation for predicting the hydraulic conductivity of  
525 unsaturated soils 1. *Soil science society of America journal*, 44(5), 892-898.
- 526 Wheeler, S. J., Sharma, R. S., & Buisson, M. S. R. (2003). Coupling of hydraulic hysteresis and  
527 stress–strain behaviour in unsaturated soils. *Géotechnique*, 53(1), 41-54.
- 528 Wheeler, S. J., & Sivakumar, V. (1995). An elasto-plastic critical state framework for unsaturated  
529 soil. *Géotechnique*, 45(1), 35-53.
- 530 Zhao, H. F., & Zhang, L. M. (2014). Effect of coarse content on shear behavior of unsaturated coarse  
531 granular soils. *Canadian geotechnical journal*, 51(12), 1371-1383.
- 532 Zhou, A., Wu, S., Li, J., & Sheng, D. (2018). Including degree of capillary saturation into constitutive  
533 modelling of unsaturated soils. *Computers and Geotechnics*, 95, 82-98.